*J. Fluid Mech.* (1980), *vol.* 96, *part* 1, *pp.* 1–26
*Printed in Great Britain*



# On flow through furrowed channels. Part 1. Calculated flow patterns

By IAN J. SOBEY

Department of Engineering Science, Oxford University

(Received 20 November 1978 and in revised form 12 April 1979)

Bellhouse *et al.* (1973) have developed a high-efficiency membrane oxygenator which utilizes pulsatile flow through furrowed channels to achieve high mass transfer rates. We present numerical solutions of the time-dependent two-dimensional Navier–Stokes equations in order to show the structure of the flow. Experimental observations which support this work are presented in a companion paper (Stephanoff, Sobey & Bellhouse 1980).

Steady flow through a furrowed channel will separate provided the Reynolds number is sufficiently large. The effect of varying the Reynolds number and the geometric parameters is given and comparisons with solutions calculated using the modern boundary-layer theory of Smith (1976) show excellent agreement. Unsteady flow solutions are given as the physical and geometric parameters are varied. The structure of the flow patterns leads to an explanation of the high efficiency of the devices of Bellhouse.

## 1. Introduction

The Navier–Stokes equations of motion of a Newtonian fluid pose a problem of overwhelming analytic difficulty, In the case of steady flows analytic solutions exist only for those flows in which the nonlinear terms either vanish or can be treated by linearization. When the fluid motion is unsteady, excepting situations in which the equations may be linearized, little is known about the structure of the solutions as the physical and geometric parameters of the problem are varied. In this paper we present details of the solution structure obtained by numerical experiments on a problem of great practical importance which nevertheless has a simple geometry: the extra-corporeal membrane oxygenator of Bellhouse *et al.* (1973). We have studied flow through this device both to understand the performance of the oxygenator and to determine the structure of solutions to the Navier–Stokes equations. Experimental observations which support this work are presented in a companion paper (Stephanoff *et al.* 1980).

Of the many life-support devices available today heart–lung machines rank amongst the most important. In cardio-pulmonary bypass some form of oxygenator is necessary to transfer oxygen into blood and remove carbon dioxide from blood. The simplest form of oxygenator is a bubble oxygenator in which oxygen is bubbled through a column of blood. Such devices have limited perfusion times because of damage caused to blood by direct contact between oxygen and blood. Longer bypass requires a membrane oxygenator in which blood is separated from oxygen by a microporous

0022-1120/80/4346-7890 $02.00 

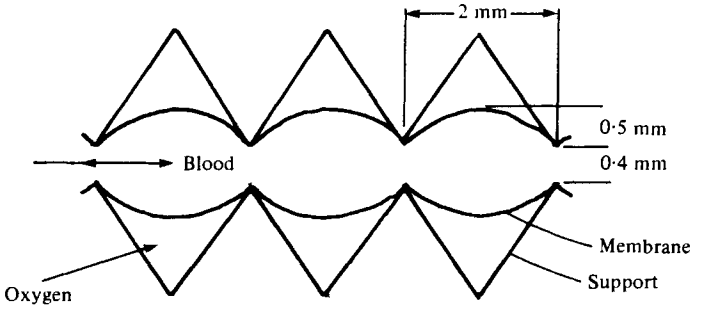


FIGURE 1. Configuration of the Oxford membrane oxygenator.

membrane. Typically the membrane thickness is of the order 40 $\mu$m with an exposed surface area of 3·5–5 m$^2$ and prime volume 500 ml.

The Oxford membrane oxygenator is built around channels formed by pressuring a membrane against a supporting structure and is shown schematically in figure 1. Blood is pumped back and forth through the channels with a small mean flow component. An oxygenator suitable for animal trials on lambs consisted of six channels of width 11·5 cm and breadth 20 cm (Bellhouse *et al.* 1973). The mean flow was 300 ml min$^{-1}$ and the effective peak volume flow could be as high as 4300 ml min$^{-1}$. As there was a large mean pressure difference between the blood side and the oxygen side of the channels, small transient pressure fluctuations that would occur during the flow cycle would not be expected to cause significant movement of the membrane. The resistance of this device was approximately 1·1 times the membrane resistance. The simple two-dimensional geometry of the blood channels means that in considering the oxygenator we must study unsteady flow through a furrowed channel. The simplest approximation is to assume that between the struts supporting the membrane the shape of the furrow is the arc of a circle. We seek to understand why such flows should generate high mass transfer rates through the membrane.

If we consider the flow of a solute from one solvent through a membrane and into another solvent then, given the concentration between solvents and the mass flow rate, the resistance to mass transfer is the ratio of driving concentration difference to mass flow rate between the solvents. The resistance is made up of three components, the membrane resistance and the fluid resistance on either side of the membrane. The fluid resistance is caused by the development of concentration gradients near the membrane which effectively result in fluid far from the membrane seeing a thicker membrane than is actually present. Clearly the resistance to mass transfer will be reduced if the fluid near the membrane is well mixed with fluid far from the membrane. In present membrane oxygenators the resistance is nearly all due to the fluid.

The device of Bellhouse is important for blood because it is able to significantly reduce the fluid resistance without using turbulent flow, but rather by using unsteady laminar flow which will not damage formed elements in the blood.

In order to avoid considering the complicated problem of blood viscosity we shall assume that the fluid flowing through the channels is a Newtonian fluid. This assumption is supported by the following:

(1) the channels are relatively wide (0·4–0·9 mm);

(2) the flow is unsteady;

(3) lateral mixing will ensure that red cells are evenly distributed through the fluid.

The unsteady part of the flow dominates the steady part and we shall generally consider oscillatory flow although the influence of mean flow components is given in § 5.

Denote the channel half-width $h$, the peak velocity assuming a flat profile $V_0$, the fluid viscosity $\nu$ and the frequency of oscillation $\Omega$. There are three interrelated parameters which govern the flow, the pulsatile Reynolds number

$$\alpha^2 = \Omega h^2/\nu,$$

the Strouhal number

$$St = \Omega h/V_0,$$

and the peak Reynolds number

$$Re = V_0 h/\nu.$$

These are related by $\alpha^2 = ReSt$. In the Oxford membrane oxygenator the ranges are $\alpha^2 = O(1)$, $St = O(10^{-2})$ and $Re = O(100)$. From a fluid-dynamic viewpoint the flow through the oxygenator is best characterized as a two-dimensional unsteady internal bluff-body problem at intermediate Reynolds number. There is little information in the literature dealing with this complicated flow regime. In order to deal with this problem we have solved a finite-difference analogue of the Navier–Stokes equations of motion for a two-dimensional flow. We have used a standard stream function/vorticity formulation (Roache 1972) taking second upwind differences for the nonlinear terms and a two time-level Dufort–Frankel substitution for the time-dependent terms. The resulting solutions were calculated on a purpose-bought PDP 11–34 computer. Our main objective has been the solution of an otherwise intractable problem using well-known numerical techniques.

In § 2 we give mathematical details of the problem and the numerical formulation. In § 3 we consider the steady flow through a furrowed channel, varying the Reynolds number and the geometric parameters. Solutions to the modern boundary-layer theory of Smith (1976) for internal flows are compared with solutions to the steady Navier–Stokes equations and excellent agreement is obtained under suitable circumstances including the size and positions of the separated region, a demonstration of the impressive power of modern boundary-layer analysis when dealing with steady flows. Studies of the unsteady problem are presented in § 4 and application of this work to the design of mass transfer devices is given in § 5 and our concluding remarks are in § 6.

## 2. Formulation

Let $(\hat{x}, \hat{y})$ be a two-dimensional Cartesian co-ordinate system and consider a channel of infinite length whose boundaries are given by

$$\hat{y} = \pm hf(\hat{x}/h),$$

where $f$ is a periodic function with

$$f(\hat{x}/h + L) = f(\hat{x}/h),$$

for all $\hat{x}$. Suppose that $f$ is a well-behaved function at least twice differentiable piecewise. A fluid of kinematic viscosity $\nu$ flows through the channel with flux $\hat{Q}$ (figure 2).

Let

$$\hat{Q} = 2Q_{\max} q(\Omega \hat{t}),$$

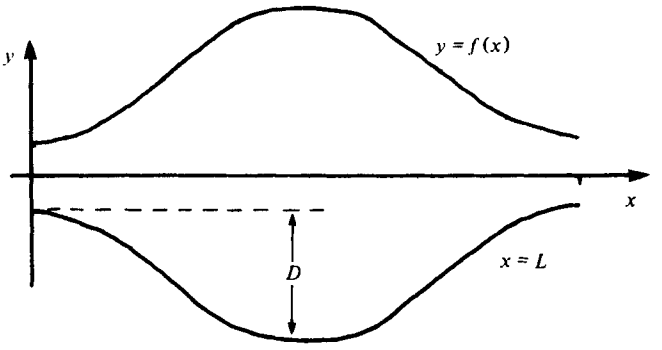


FIGURE 2. Geometry of a furrowed channel.

where $q$ is a function with period $2\pi$, $|q| \leqslant 1$ and $\hat{t}$ is the time. We define a channel velocity by

$$V_0 = Q_{\max}/h,$$

and suppose $(\hat{u}, \hat{v})$ are the velocities in the $(\hat{x}, \hat{y})$ directions respectively. The vorticity $\hat{\omega}$ is defined by

$$\hat{\omega} = \partial\hat{v}/\partial\hat{x} - \partial\hat{u}/\partial\hat{y}.$$

We shall say that the flow is accelerating if $q > 0$ and $\dot{q} > 0$ or $q < 0$ and $\dot{q} < 0$; and that the flow is decelerating otherwise. The vorticity equation is

$$\frac{\partial\hat{\omega}}{\partial\hat{t}} + \hat{u}\frac{\partial\hat{\omega}}{\partial\hat{x}} + \hat{v}\frac{\partial\hat{\omega}}{\partial\hat{y}} = \nu\hat{\nabla}^2\hat{\omega},$$

where

$$\hat{\nabla}^2 = \partial^2/\partial\hat{x}^2 + \partial^2/\partial\hat{y}^2.$$

In addition the continuity equation is

$$\partial\hat{u}/\partial\hat{x} + \partial\hat{v}/\partial\hat{y} = 0.$$

These equations, together with the boundary conditions

$$(\hat{u}, \hat{v}) \equiv (0, 0) \quad \text{on} \quad \hat{y} = \pm hf(\hat{x}/L),$$

and the condition that the flux is a given function of time, completely specify the problem. In order to obtain a finite-difference analogue we first transform the equations by means of the transformation

$$x = \hat{x}/h,$$
$$z = \hat{y}/hf(\hat{x}/L),$$
$$t = \Omega\hat{t},$$

and the scaling

$$\hat{u} = \frac{Q_{\max}}{hf(x)}\frac{\partial\psi}{\partial z},$$

$$\hat{v} = -\frac{Q_{\max}}{h}\left[\frac{\partial\psi}{\partial x} + \frac{p'}{p}z\frac{\partial\psi}{\partial z}\right],$$

where for convenience $p(x) = 1/f(x)$. The vorticity is scaled

$$\hat{\omega} = \frac{Q_{\max}}{h^2}\omega,$$

whence

$$\omega = -\nabla^2\psi,$$

where

$$\nabla^2 = \frac{\partial^2}{\partial x^2} + \left(p^2 + \left(\frac{p'}{p}\right)^2 z^2\right)\frac{\partial^2}{\partial z^2} + \frac{2p'z}{p}\frac{\partial^2}{\partial x\,\partial z} + \left[\left(\frac{p'}{p}\right)' + \left(\frac{p'}{p}\right)^2\right]z\frac{\partial}{\partial z}.$$

The vorticity equation is

$$\frac{\partial\omega}{\partial t} = -\frac{1}{St}\left[\frac{\partial(u\omega)}{\partial x} + \frac{p'z}{p}\frac{\partial(u\omega)}{\partial z} + p\frac{\partial}{\partial z}(v\omega)\right] + \frac{1}{\alpha^2}\nabla^2\omega,$$

and the boundary conditions

$$\psi|_{z=\pm 1} = \pm q(t),$$

and

$$\psi_z = \psi_x \equiv 0 \quad \text{on} \quad z = \pm 1.$$

In order to model these equations numerically we follow the philosophy of Gillani & Swanson (1976) and use a fine mesh near the wall $z = 1$ and a coarse mesh near $z = 0$. The problem is symmetric about $z = 0$ and we have a computational region $0 \leqslant z \leqslant 1$ and $0 \leqslant x \leqslant L$. The boundary conditions at $x = 0$ and $x = L$ are given by the periodic nature of the wall,

$$\psi|_{x=0} = \psi|_{x=L}$$

and

$$\omega|_{x=0} = \omega|_{x=L}.$$

This is the only novel point from the numerical view. Usually some approximation is necessary in order to specify the entrance and exit conditions. Here no approximation is involved: the calculation is iterated until the entrance and exit conditions match.

The numerical technique used to solve the equations is well known and has been widely used. Essentially, if the field is known at time $t$, the vorticity equation is used to estimate the vorticity at a later time $t + \delta t$, where $\delta t$ is a small time interval. A Poisson equation is then solved for the stream function at the new time and the procedure repeated. In order to increase the stability of the difference equations the nonlinear terms are treated by a second upwind differencing technique. This is really a statement of the Cauchy–Kelvin–Helmholtz law that vortex lines move with the fluid and, instead of taking space derivatives at a point in the nonlinear terms, they are taken slightly upstream. The vorticity is stored at two time levels and a Dufort–Frankel substitution is made in the time derivative and viscous terms. These techniques are well described by Roache (1972). Our fine mesh contained 410 points and the coarse mesh 210. This mesh size restricted the non-dimensional time step to $10^{-4}$ to $10^{-2}$ depending on $\alpha^2$ and $St$. The solutions were obtained on a PDP 11-34 computer and a typical run from $t = 0$ until $t = 1{\cdot}5$ would take about 5–10 hours. In those cases where the flow is inertially dominated the solution for $t = 0{\cdot}5$ until $t = 1{\cdot}5$ would be an accurate sample of a general cycle. If viscous effects dominated there would still be asymmetry in the time cycle due to the starting conditions (the flow starts from rest but thereafter at the instant of zero mean flow there is considerable motion in the fluid). Calculations were performed using single-precision arithmetric as comparison runs using double precision had shown no appreciable improvement in accuracy. The Poisson equation for the stream functions was solved by using pointwise over-relaxation. Our aim was

the systematic study of the fluid dynamics and having obtained a mesh size that worked we have not performed calculations involving variation of the numerical parameters, rather we have concentrated on variation of the physical parameters. We also have a variation of the program in which the nonlinear terms are deleted. This enables solutions of the unsteady Stokes equations to be obtained. Comparison of the Stokes solutions with the full solutions is useful in showing whether inertial effects are important.

One point of uncertainty in numerical calculations has been the treatment of boundary vorticity at a corner. Roache (1972) details several different methods that have been used. Following a suggestion by Lighthill (1977, private communication) we considered a boundary shape given by

$$f(x) = 1 + \tfrac{1}{2}D(1 - \cos(2\pi x/L))$$

and a boundary shape given by

$$f(x) = \begin{cases} 1 & 0 < x < \tfrac{1}{2}x_w, \quad L - \tfrac{1}{2}x_w < x < L, \\ \text{arc of a circle} & x_w/2 < x < L - x_w/2, \end{cases}$$

where $x_w$ represents the strut width which has adjusted so that the corners did not fall at a grid point. In both cases the fundamental structure of the flow field was the same. The later case is relevant to the oxygenator design and the results in § 5 are for this boundary shape. The results in § 3 and § 4 are for the sinusoidal geometry. Further in both cases the point about which the length $L$ and depth $D$ are varied is taken to be that of the oxygenator; $L = 8$, $D = 2$.

In order to have an idea of the strength of the vortex in the furrow we have defined the vortex strength to be the difference between the maximum value of the stream function and the value at the wall (or minimum if the wall stream function value is negative).

## 3. Steady flow

We use two different methods to obtain solutions for steady flow through a furrowed channel. In § 3.1 we present numerical solutions of the Navier–Stokes equations. These solutions were obtained by solving the unsteady equations with constant boundary conditions. In particular the boundary condition on the stream function was

$$\psi|_{z=1} = \begin{cases} \sin 2\pi t & 0 < t < 0{\cdot}25, \\ 1 & t \geqslant 0{\cdot}25. \end{cases}$$

Thus we imposed a gradual acceleration to peak flow conditions and subsequently kept the flux through the channel constant. In § 3.2 we use the method of Smith (1976) to obtain an approximate solution that is valid in the limits of large Reynolds number and small change in channel width. We have compared the two solutions both to verify the numerical solution and to confirm the applicability of Smith's analysis.

### 3.1. *Numerical solution of the steady equations of motion*

Consider a sinusoidally varying wall shape where the furrows have physical dimensions $L = 8$ and $D = 2$. At low Reynolds number the flow does not separate and the fluid streams through the hollow, largely following the wall shape (see figure 3*a*). As

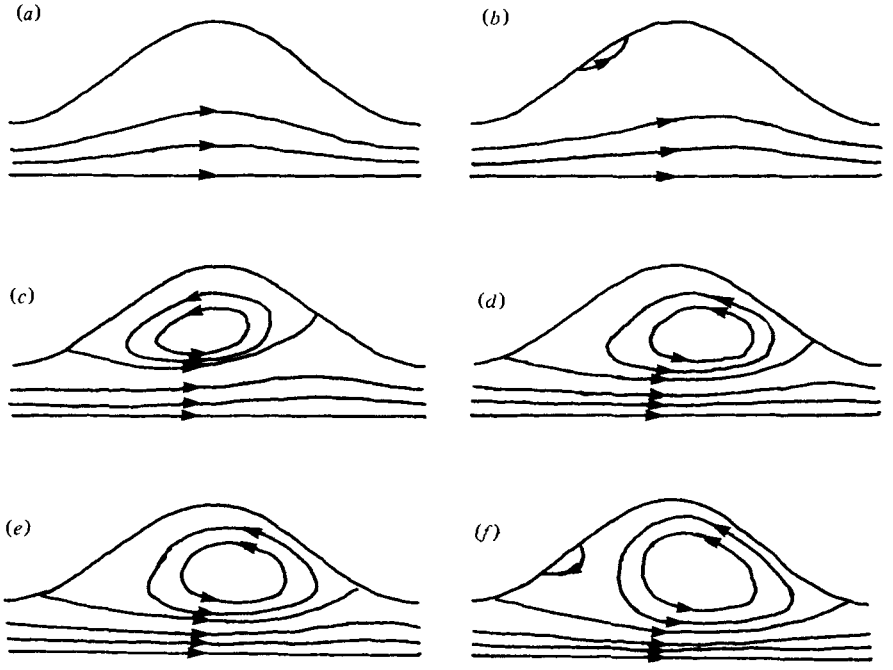


FIGURE 3. *Streamlines for steady flow as the Reynolds number varies. (a) Re = 0; (b) Re = 5; (c) Re = 15; (d) Re = 75; (e) Re = 150; (f) Re = 600.*

the Reynolds number increases, inertial effects become important until at $Re = 5$ a small separated region exists midway along the upstream wall of the hollow (figure 3*b*). Further increases in the Reynolds number cause the separated region to enlarge until at $Re = 15$ it fills the major part of the hollow (figure 3*c*). At larger Reynolds numbers the vortex grows further, the centre shifts downstream in the hollow and the vortex bulges into the mainstream. At even higher Reynolds numbers the vortex will separate from the upstream wall and a small counter-rotating vortex forms on that wall (figure 3*e*). The occurrence of a second counter-rotating vortex has been predicted by Snuggs (1977) for a semi-cylindrical hollow.

In figure 4 we show the variation of the boundary vorticity with Reynolds number. At zero Reynolds number the vorticity is symmetrically distributed about the hollow centre. As the Reynolds number increases the vorticity decreases in the upstream section of the hollow and separation occurs. As the separation region increases in size a marked peak occurs in the vorticity at the wall in the hollow. A spatial oscillation in the wall vorticity occurs on the upstream wall and eventually this leads to separation of the vortex. The maximum vorticity occurs just before the end of the hollow. The maximum value of the stream function is shown in figure 5. As the Reynolds number increases from 5 to 30 there is a rapid increase in the stream function maximum but thereafter the rate of increase drops.

If the hollow length is varied whilst the depth is kept constant the maximum value of the stream function increases at first, but near $L = 10$ there is a small maximum in the vortex strength (figure 6). At large $L$ we do not expect a separated region, and we show below that modern boundary-layer theory predicts this, and thus there will be a decrease in the vortex strength as $L$ increases. Varying the hollow depth whilst

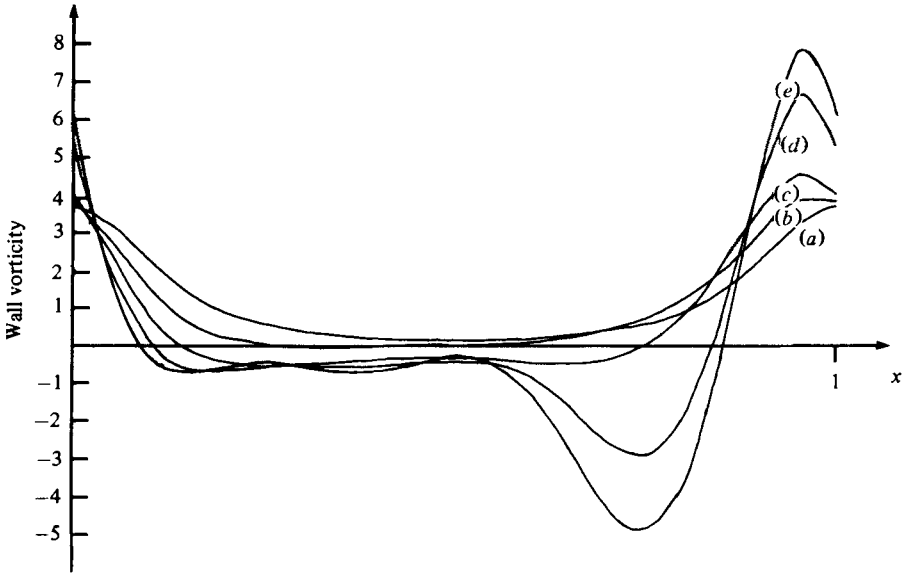


FIGURE 4. Variation of wall vorticity with Reynolds number. (*a*) $Re = 0$; (*b*) $Re = 5$; (*c*) $Re = 15$; (*d*) $Re = 75$; (*e*) $Re = 150$.

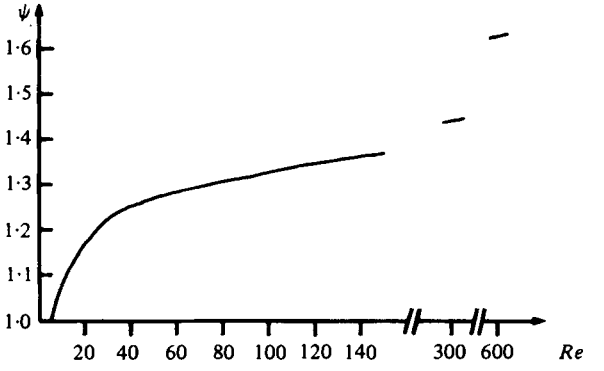


FIGURE 5. Variation of stream function maximum with Reynolds number in steady flow with $L = 8$ and $D = 2$.

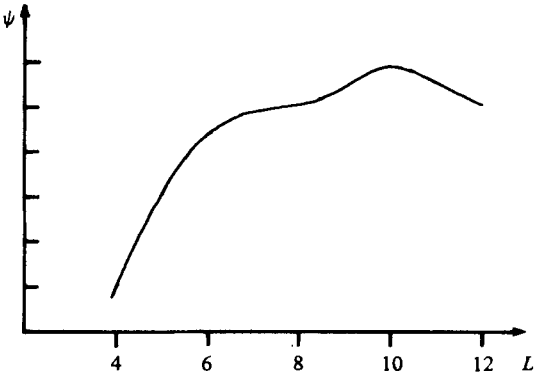


FIGURE 6. Stream function maximum *versus* furrow length in steady flow with $D = 2$ and $Re = 75$.

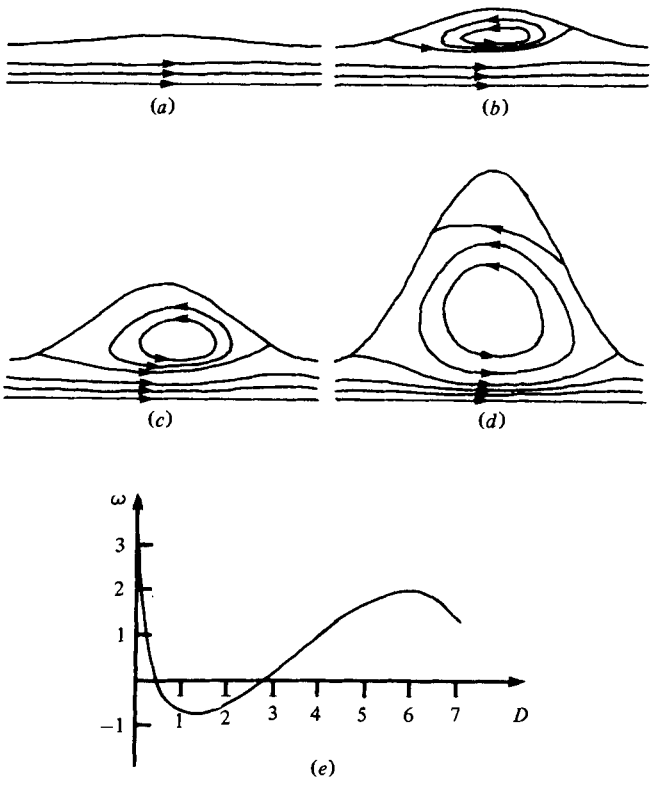


FIGURE 7. Effects of hollow depth on steady flow. (*a*) $D = 0{\cdot}25$; (*b*) $D = 1$; (*c*) $D = 2$; (*d*) $D = 5$; (*e*) vorticity at apex of furrow as $D$ varies. All calculated at $Re = 75$ and $L = 8$.

keeping the length constant leads to a second (and third, etc.) vortex occuring in the deepest part of the hollow. In figure 7 we show the streamlines for $D$ varying between $\frac{1}{4}$ and 5. The second vortex appears at $D = 2{\cdot}8$; in figure 7 (*e*) we show the variation of boundary vorticity at the apex of the hollow, and this shows the occurrence of a second (and presumably third, etc.) vortex in the deepest part of the hollow.

The behaviour of the boundary vorticity as the hollow depth increases is shown in figure 8. For small $D$ the separated region is absent, first appearing at $D \approx 0{\cdot}4$. The second vortex is indicated by positive vorticity near the centre of the hollow.

### 3.2. *Modern boundary-layer solution*

A great advance in boundary-layer theory was achieved by Stewartson & Williams (1969) who showed that if a correct ratio of longitudinal to lateral length scales was chosen then it was possible to analyse disturbances to a boundary layer. Recently Smith in a series of papers (e.g. Smith 1976) has shown how the ideas of Stewartson & Williams may be applied to internal flows. Although in the classical sense there is no boundary layer at the walls in an internal flow, Smith has shown that the Navier–Stokes equations may be reduced to a boundary-layer equation. Even though the triple deck structure of Stewartson and Williams has been lost the underlying philosophy, the correct choice of lateral and longitudinal length scales, remains. In this section we present solutions to the equations developed by Smith and compare them to solutions of the full Navier–Stokes equations.

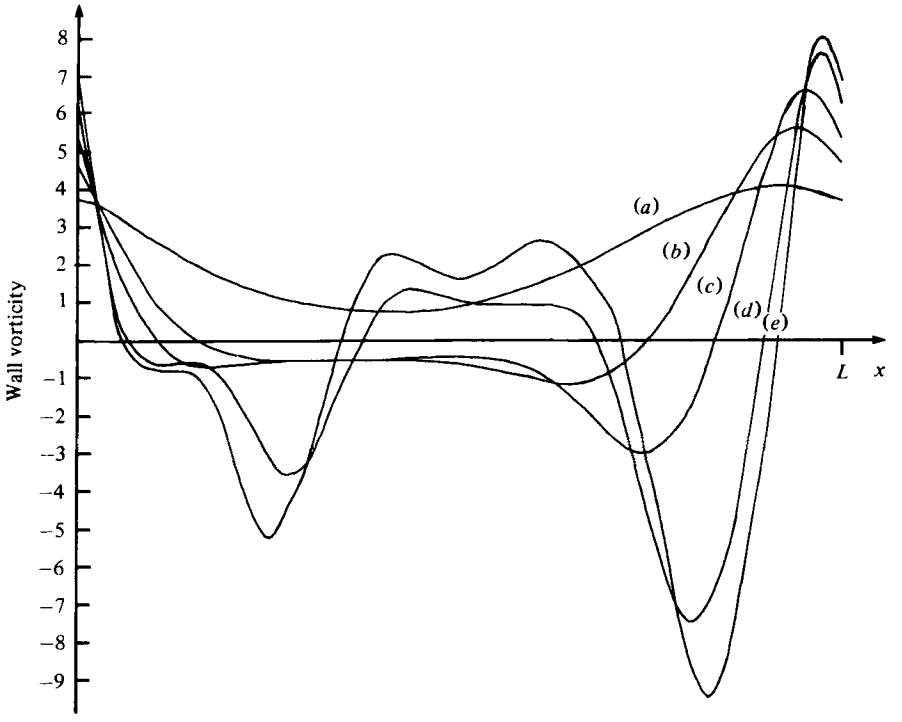


FIGURE 8. Wall vorticity as furrow depth increases. (*a*) $D = 0{\cdot}25$; (*b*) $D = 1$; (*c*) $D = 2$; (*d*) $D = 5$; (*e*) $D = 6$.

In the symmetric channel Smith (1976) has shown that we should consider the boundary to be perturbed on a scale $Re^{-\frac{1}{2}}\epsilon^{-\frac{1}{2}}h$ in the $\hat{x}$ direction and $Re^{-\frac{1}{2}}\epsilon^{-\frac{1}{2}}h$ in the $\hat{y}$ direction, where $\epsilon = o(Re^{-\frac{1}{3}})$. There will be two regions of interest, a core flow in which $0 < z \ll 1$, and a viscous layer adjacent to the wall, $1-y = O(\epsilon^{-\frac{1}{2}}Re^{-\frac{1}{2}})$ where $y = \hat{y}/h$. A symmetrically indented channel leaves the core velocities unperturbed to first order whilst the pressure has a perturbation of $O(\epsilon^{-1})$. The pressure perturbation will be independent of the lateral variable ($y$) and depend only on the longitudinal one ($x$). Define the scalings

$$x = Re^{-\frac{1}{2}}\epsilon^{-\frac{3}{2}}\xi$$

and

$$1-y = Re^{-\frac{1}{2}}\epsilon^{-\frac{1}{2}}\zeta;$$

then Smith (1976) has shown that the solution near the wall has leading-order terms

$$u = Re^{-\frac{1}{2}}\epsilon^{-\frac{1}{2}}U(\xi, \zeta),$$

$$v = Re^{-\frac{1}{2}}\epsilon^{\frac{1}{2}}V(\xi, \zeta),$$

$$p = \epsilon^{-1}P(\xi).$$

$U$, $V$ and $P$ satisfy the equations

$$\frac{\partial U}{\partial \xi} + \frac{\partial V}{\partial \zeta} = 0,$$

and

$$U\frac{\partial U}{\partial \xi} + V\frac{\partial U}{\partial \zeta} = -P'(\xi) + \frac{\partial^2 U}{\partial \zeta^2},$$

together with the boundary conditions

$$U = V \equiv 0 \quad \text{on} \quad \zeta = HF(\xi),$$

where $F$ is given by the boundary shape

$$\hat{y} = \pm Re^{-\frac{1}{4}}\epsilon^{-\frac{3}{8}}Hh\,F(\xi)$$

and in this case is a periodic function

$$F(\xi) = F(\xi + n)$$

for integer $n$, and

$$U \to \tfrac{3}{2}\zeta \quad \text{as} \quad \zeta \to \infty.$$

We replace the condition of Smith regarding $\partial U/\partial\zeta$ as $\xi \to -\infty$ with a periodicity condition. We also note that, in the core, the unperturbed flow is

$$u \sim \tfrac{3}{2}(1-y^2),$$

as we have chosen in § 2 to have unit flux through each half channel. Apart from these minor points the formulation follows Smith (1976).

A method of solution of the boundary-layer equations has been given by Smith (1974) and we have used that method to obtain solutions, starting from $U = \frac{3}{2}\zeta$ at $\xi = 0$ and marching forward in the $\xi$ direction. We found the solution in only the second hollow closely satisfied the periodicity condition, demonstrating the lack of upstream influence in symmetrically indented channels. Using the sinusoidal boundary geometry of § 2 we have

$$F(\xi) = \tfrac{1}{2}(1 - \cos 2\pi\xi),$$

and the physical parameters are given by

$$D = \epsilon^{-\frac{1}{2}}Re^{-\frac{1}{4}}H,$$

$$L = \epsilon^{-\frac{3}{8}}Re^{-\frac{1}{4}}H,$$

whence

$$|H| = D\,Re^{\frac{1}{8}}L^{-\frac{1}{8}} \quad \text{and} \quad \epsilon = Re^{-\frac{1}{3}}L^{-\frac{8}{3}}.$$

We have compared the two solutions, boundary-layer and full numerical, at $Re = 75$, a relatively large intermediate Reynolds number. Choosing $L = 8$ then $\epsilon = 0{\cdot}06$ whilst $H = 2{\cdot}1358D$. In figure 9 we show the boundary vorticity calculated from the two solutions for hollows of depth $\frac{1}{4}$ and $\frac{1}{2}$. Figure 10 compares the streamlines for the later case. The agreement is striking and the boundary-layer theory predicts the qualitative features of the flow very well. This can only increase the confidence one feels in using the theories of Smith. In this example our calculations show that separation occurs if

$$Re^{\frac{1}{8}}L^{-\frac{1}{8}}D > 0{\cdot}795,$$

i.e. if the Reynolds number is large, the hollow short or deep, all of which agrees with our physical intuition. Further for the case $Re = 75$, $L = 8$ this theory gives separation if $D > 0{\cdot}38$. In our solutions to the steady Navier–Stokes equations we found a separated region existed if $D \approx 0{\cdot}4$, and thus excellent agreement is obtained between the two solutions.

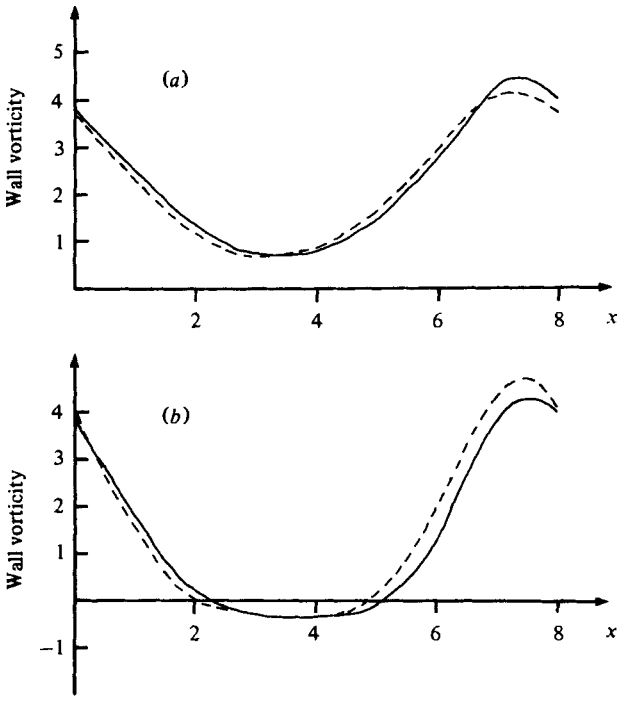


FIGURE 9. Comparison of wall vorticity calculated from asymptotic theory of Smith (——) and from numerical solution of steady Navier–Stokes equations (– – –) at a Reynolds number of 75. (*a*) $D = 0{\cdot}25$; (*b*) $D = 0{\cdot}5$.

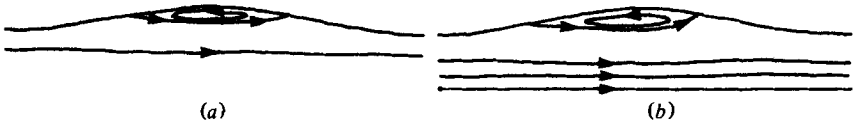


FIGURE 10. Comparison of streamlines at $Re = 75$ calculated: (*a*) using the theory of Smith; (*b*) from the Navier–Stokes equations.

## 4. Unsteady flow

Unsteady flow through a furrowed channel can be characterized by at least five parameters, the pulsatile Reynolds number ($\alpha^2$), the Strouhal number ($St$), the hollow length ($L$), depth ($D$) and the time history of the flow. We shall assume that the flow starts from rest and develops as an oscillatory flow. On the boundary $z = 1$ the streamfunction is given by

$$\psi = \sin 2\pi t.$$

In this case we are left with two physical parameters, the pulsatile Reynolds number and the Strouhal number and two geometric parameters, the length and depth of the furrow. As in the steady flow case we chose to vary $L$ and $D$ about the values characteristic of the oxygenator. One other point concerns notation. Historically separation refers to a separated boundary layer. We choose a slightly different meaning and say that if at any point the wall vorticity has opposite sign to the flux through the channel, the flow has separated. As we show below separation in this sense may occur when

either inertial or viscous effects dominate and in an external flow one would refer to a separated boundary layer or a reversing Stokes layer. This definition of separation allows us to define a global parameter, the time of separation of the flow.

### 4.1. *Structure of the flow cycle*

Previous experiments by Bellhouse *et al.* (1973) and Bellhouse & Snuggs (1977) have shown that vortices are observed in furrowed channels. Snuggs (1977) observed visually with the aid of small particles that during an acceleration from rest a vortex could be set up in a semicircular hollow adjacent to a semi-infinite region. During a subsequent deceleration to rest he observed that the vortex violently expanded out of the hollow, the flow nevertheless remaining laminar. Stephanoff *et al.* (1980) have also observed vortex motion in furrowed channels and considered the conditions in which vortices are established in the furrows. In this section we shall present a generalized view of the flow pattern assuming a vortex is set up in the furrow. Subsequently to the calculations of this section Stephanoff *et al.* (1980) have shown using photographs of particle paths that the patterns presented here are indeed observed. We defer until later the consideration of those flows which do not result in a vortex forming in the furrow.

At the start of an acceleration from rest the fluid streams through the channel following the wall shape. In the vicinity of the upstream wall there will be two major influences on the fluid motion. The expansion of the channel cross-section and the resulting deceleration of the fluid will cause a pressure gradient which opposes the fluid motion. Acceleration of the fluid results in a pressure gradient in the opposite sense. Initially the acceleration will control the pressure gradient and prevent separation but because the total flux continues to increase and the acceleration rate decreases separation may occur. This can be illustrated by ignoring any vorticity present in the free stream and considering unsteady irrotational flow through a channel. If the irrotational flow potential per unit volume flux were $\Phi(x, y)$, then the potential with volume flux $q(t)$ would be $q(t)\,\Phi(x, y)$ and the pressure gradient along the wall would be

$$-St\dot{q}\frac{\partial\Phi}{\partial s}-q^2\frac{\partial\Phi}{\partial s}\frac{\partial^2\Phi}{\partial s^2}.$$

The first term is negative for an accelerating flow and the second term is positive in a region of expanding cross-section. Hence separation would not occur provided

$$St\dot{q} > -q^2\frac{\partial^2\Phi}{\partial s^2}.$$

See, for example, Lighthill (1963) who showed that the pressure gradient is the vorticity source strength and that separation is impossible where the vorticity source strength is positive but tends to occur shortly after the vorticity source strength becomes negative. This suggests that the ratio

$$S = St\dot{q}/(-q^2\Phi_{ss})$$

should everywhere satisfy a criterion $S > S_{\mathrm{crit}}$, where $S_{\mathrm{crit}}$ is a bit less than 1, if separation is to be avoided.

As the acceleration rate decreases and the flow rate increases this condition would

not be met and an adverse pressure gradient would occur at the wall causing the flow to separate. The separated region increases in size during the remainder of the acceleration and during the deceleration continues to increase in size. The vortex centre moves downstream in the furrow and the vortex bulges into the mainstream. The growth of the vortex during the deceleration is somewhat surprising. Apparently it is simpler for the fluid to effectively decrease the channel gap by increasing the size of the vortex than to decrease the velocity of the bulk of the fluid. It would be interesting to demonstrate this point by considering the energy required in the two different situations! As the mainstream decelerates further the vortex continues to grow until just before the flow changes direction the fluid is flowing backwards along the wall and forwards in the centre of the channel. As the flux reverses the fluid near the wall has anticipated the flow reversal and the fluid now moves between the vortex and the wall, ejecting the vortex into the mainstream. The reversal of flow near a wall in a decelerating flow is not unusual; what is interesting is the effect on the vortex of the flow reversal. Subsequently the vortex disappears as fluid from it is gathered into the accelerating mainstream. A new separated region will then form in the furrow as the cycle continues. In inertially dominated flows such as these there appears to be little influence on the formation of the separated region by the conditions at zero mean flow.

Our calculations show that it is possible for the old ejected vortex to be still present when the new one forms. In figure 11 we show a sequence of calculated streamlines for $\alpha^2 = 0{\cdot}75$ and $St = 0{\cdot}01$ which illustrate these flow patterns. In figure 12 we show the boundary vorticity as time varies at the narrowest part of the channel and at the apex of the furrow.

### 4.2. *Time of separation*

We indicated above that we intend to use the time of separation as a global dependent parameter which characterizes the flow. If the geometric parameters are constant then the separation time ($t_s$) will be a function of the pulsatile Reynolds number and the Strouhal number,

$$t_s = t_s(\alpha^2, St).$$

In any half cycle $t_s$ will have to satisfy $0 \leqslant t_s \leqslant 0{\cdot}5$. Consider the values of $t_s$ on the lines $\alpha^2 = 0$ and $St = 0$. If the pulsatile Reynolds number vanishes then we essentially have steady Stokes flow and there will be no separation. Thus on the line $\alpha^2 = 0$ we also have $t_s = 0{\cdot}5$. If we now consider the line $St = 0$ then we have steady flow and furthermore, excepting at the point $\alpha^2 = 0$, the Reynolds number will be sufficient to cause separation. Thus the line $\alpha^2 > 0$, $St = 0$ will have $t_s = 0$. This leads us to the conclusion that the surface formed when $t_s$ is plotted against the pulsatile Reynolds number and the Strouhal number must have a singular fold near the origin. In figure 13(*a*), curve (i), we show the separation time as the Reynolds number varies for a small but finite Strouhal number ($St = 0{\cdot}01$). It can be seen that there is a rapid transition from flows which separate in the acceleration phase to those which separate in the deceleration phase. In figure 13(*b*) we show the line $t_s = 0{\cdot}25$ which divides flows that separate in the acceleration from those which separate in the deceleration. A most important point is that for Strouhal numbers which are less than 0·02 (approximately) the dividing line is straight and represents a Reynolds number of approximately 5. Stephanoff *et al.* (1980) show that this same line can be shown to divide those flows which appear to have vortices formed in the furrows from those which do not.

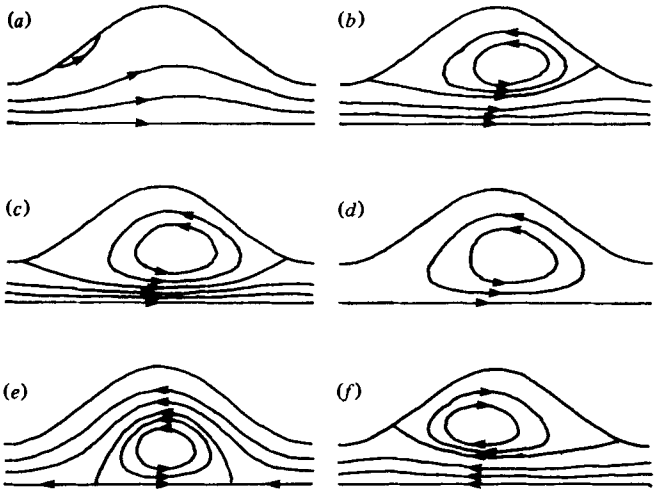


FIGURE 11. Streamlines for unsteady flow through a furrow. Calculated at $\alpha^2 = 0{\cdot}75$, $St = 0{\cdot}01$, $L = 8$ and $D = 2$. (*a*) $t = 0{\cdot}1$; (*b*) $t = 0{\cdot}25$; (*c*) $t = 0{\cdot}45$; (*d*) $t = 0{\cdot}5$; (*e*) $t = 0{\cdot}55$; (*f*) $t = 0{\cdot}75$.

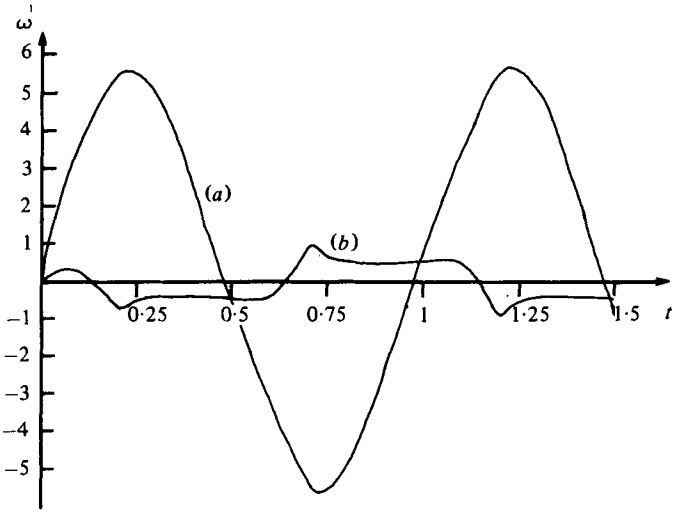


FIGURE 12. Variation of wall vorticity in unsteady flow: (*a*) wall vorticity at $x = 0$; (*b*) wall vorticity at apex of furrow. Calculated for $\alpha^2 = 0{\cdot}75$, $St = 0{\cdot}01$, $L = 8$ and $D = 2$.

In § 3 we calculated that for this geometry steady flow separates at a Reynolds number of approximately 5 and these links enable us to explain the nature of the singularity at the origin of the $\alpha^2$, $St$ plot of the separation time. At small Strouhal numbers, evidently of the order $10^{-2}$, the flow is controlled by peak Reynolds number. If the peak Reynolds number is sufficient to cause separation in the equivalent steady flow then the unsteady flow will separate some time before the instant of peak flow; otherwise the flow is dominated by viscous effects. Further, in the region of small Strouhal number at the instant of peak flow, the flow closely approximates the equivalent steady flow (that is steady flow at the peak Reynolds number). This is illustrated in figure 14 where we show the boundary vorticity for the case $\alpha^2 = 0{\cdot}75$ and $St = 0{\cdot}01$ at time $t = 0{\cdot}25$ and the case $\alpha^2 = 3$ and $St = 0{\cdot}04$ at time $t = 0{\cdot}25$. In both cases the

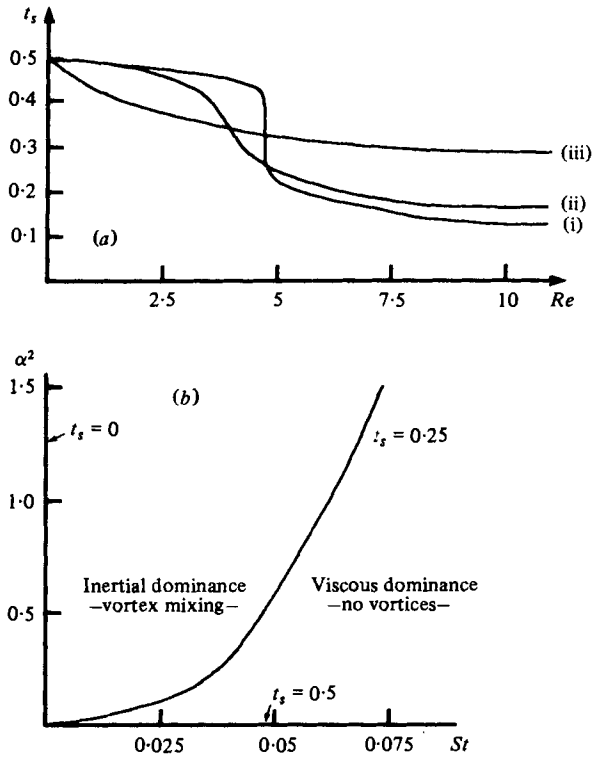


FIGURE 13. (*a*) Variation of time of separation with pulsatile Reynolds number for (i) $St = 0{\cdot}01$, (ii) $St = 0{\cdot}02$, (iii) $St = 0{\cdot}1$. (*b*) Dividing line between flows that separate in the acceleration ($t_s < 0{\cdot}25$) and those that separate in the deceleration ($t_s > 0{\cdot}25$).

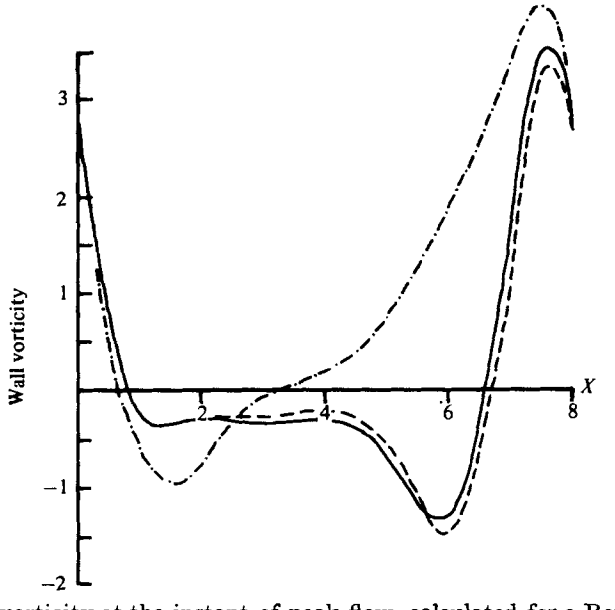


FIGURE 14. Wall vorticity at the instant of peak flow, calculated for a Reynolds number of 75 and hollow depth 2. ——, $St = 0{\cdot}01$; – · – · –, $St = 0{\cdot}04$; – – –, steady calculation.

instantaneous Reynolds number is 75. Comparison with the steady flow at Reynolds number of 75 shows that indeed close agreement exists at small Strouhal numbers between the steady flow and the unsteady peak flow. This behaviour indicates that at small Strouhal numbers the flow has some quasi-steady characteristics. The occurence of separation is dependent only on a critical Reynolds number and at the instant of peak flow the flow closely resembles the steady flow solution. However, there are some features which cannot be described by quasi-steady theory. During the deceleration the vortex grows in size. A naive use of quasi-steady theory would indicate that the vortex should *decrease* in size as the mainstream decelerates. This does not happen. To examine the nature of the flow development during the acceleration we return to the ideas of § 4.1. There it was shown that quasi-steady potential theory predicted the inhibition of separation when

$$S > S_{\text{crit}}$$

and where $S_{\text{crit}}$ is a little less than one. In the case of a slender channel of length $L$ and depth $D$ we can approximate the potential velocities by

$$u \sim \frac{1}{f} + \frac{y^2}{2}\left(\frac{f'}{f^2}\right)' + O\left(\left(\frac{D}{L}\right)^4\right),$$

and

$$v \sim \frac{yf'}{f^2} + O\left(\left(\frac{D}{L}\right)^3\right).$$

These estimates are very crude but as we shall show they are sufficient for our purposes. The velocity along the wall is given by

$$\tilde{q} = (u^2 + v^2)^{\frac{1}{2}},$$

thus

$$\tilde{q} \sim \frac{1}{f}\left[1 + \tfrac{1}{2}(ff'' - f'^2)\right] + O\left(\left(\frac{D}{L}\right)^4\right).$$

The arc length along the wall is

$$s = \int_0^x (1 + f'^2)\, dx,$$

and hence, using

$$\Phi_{ss} = \frac{\partial \tilde{q}}{\partial x} \Big/ \frac{\partial s}{\partial x},$$

we obtain

$$\Phi_{ss} \sim -\frac{f'}{f^2}\left[1 - \frac{1}{2}\frac{f^2 f'''}{f'} + ff'' - f'^2\right].$$

Using the results of our numerical experiments we have calculated the value of $S$ as the Strouhal number and the Reynolds number vary. The values are shown in table 1. The values of $S$ should be treated with some caution as the discrete nature of the grid only allows approximate determination of the position of separation. It can be seen that at low Strouhal numbers the value of $S$ at which separation occurs is remarkably constant (and less than 1) and this supports the idea that at small Strouhal numbers the flow initially develops in a quasi-steady manner. We have also shown that as $\dot{q} \to 0$ (peak flow) the instantaneous unsteady solution tends to the steady solution at the peak Reynolds number. This allows us to conjecture that the flow is indeed

| | | | | | |
|---|---|---|---|---|---|
| $Re = 75$ | | | | | |
| $St$ | 0·001 | 0·005 | 0·01 | 0·02 | 0·04 |
| $Re_s$ | 15·4 | 31·1 | 42·2 | 55·3 | 68·3 |
| $X_s$ | 1·9 | 1·7 | 1·6 | 1·5 | 1·4 |
| $S$ | 0·66 | 0·61 | 0·57 | 0·49 | 0·37 |
| $Re = 30$ | | | | | |
| $St$ | 0·001 | 0·005 | 0·01 | 0·02 | 0·04 |
| $Re_s$ | 7·9 | 13·6 | 17·9 | 22·9 | 27·8 |
| $X_s$ | 2·2 | 1·9 | 1·8 | 1·7 | 1·6 |
| $S$ | 0·59 | 0·61 | 0·57 | 0·51 | 0·38 |
| $St = 0{\cdot}01$ | | | | | |
| $Re$ | 6 | 30 | 75 | 100 | 150 |
| $Re_s$ | 5·5 | 17·9 | 42·2 | 55·2 | 82·0 |
| $X_s$ | 2·2 | 1·8 | 1·6 | 1·5 | 1·5 |
| $S$ | 0·43 | 0·57 | 0·57 | 0·54 | 0·55 |

TABLE 1. Computed values of the Reynolds number at separation $Re_s$, the position of separation ($X_s$) and the function $S$ for a hollow of length $L = 8$ and depth $D = 2$.

developing throughout the cycle in a quasi-steady manner. Thus even though we cannot at present write down an analytic description of a quasi-steady separated flow, there are two *separate* influences on the development of the vortex, one behaving like $q$ and representing the unsteady effects and another related in some unknown fashion to the equivalent steady solution.

As the Strouhal number increases the 'singularity' in the time of separation surface decreases and this can be seen in curves (ii) and (iii) of figure 13(*a*) where we show the variation of $t_s$ with Reynolds number. For Strouhal numbers of the order 0·1 and larger the flow *never* separates in the acceleration phase. This means that at these Strouhal numbers the viscous terms in the equations are of sufficient importance to dominate the nonlinear inertial terms even at high Reynolds number. As the Strouhal number becomes very large we will obtain the unsteady Stokes solutions and the calculations presented in § 4.4 indicate that for Stokes flows separation always occurs late in the deceleration and never in the acceleration.

### 4.3. *Variation of the geometric parameters*

In addition to the two physical parameters there are two geometric parameters, the furrow length $L$ and depth $D$. In § 3 we demonstrated that in steady flow it is possible to have successive vortices in deep furrows. This is also true if the flow is unsteady. Separation occurs further upstream than in a shallow furrow, a result of the increased width of the channel. The separated region enlarges and a primary vortex is formed in the furrow. The primary vortex then separates from the downstream wall near the apex of the furrow forming a secondary counter-rotating vortex at the apex of the furrow (see figure 15). As the mainstream decelerates the primary vortex enlarges and as the flow reverses is ejected from the furrow whilst the secondary vortex remains at the apex of the furrow. Viscous action then causes the secondary vortex to enlarge as the mainstream accelerates. The original vortex is eliminated as fluid from it is taken up by the mainstream. The vortex in the furrow then separates near the apex of the furrow and the pattern repeats itself.

If the hollow length is varied we again find a small maximum in the vortex strength

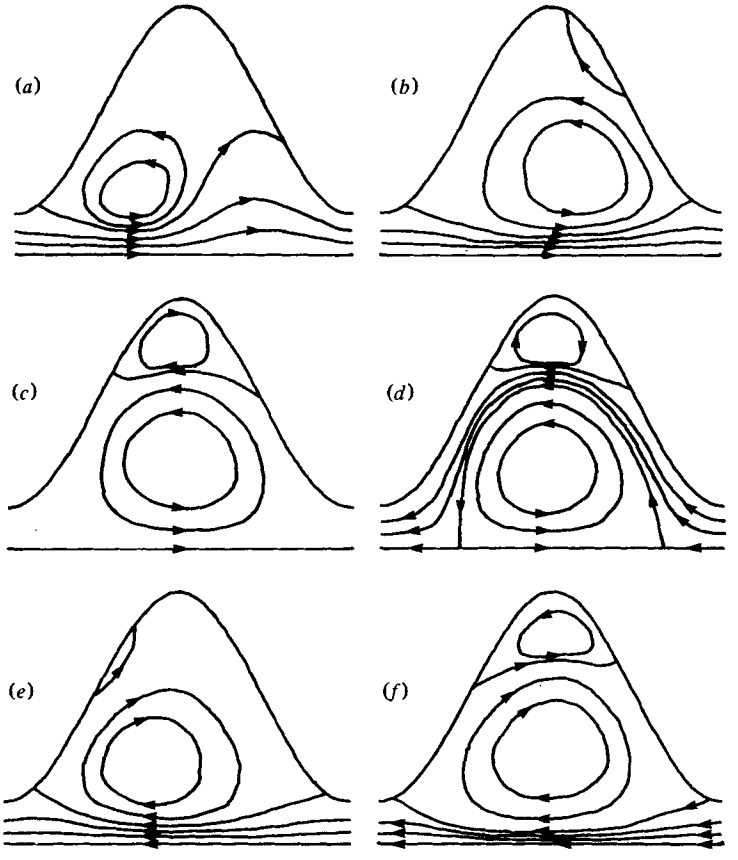


FIGURE 15. Streamlines for unsteady flow through a deep hollow, calculated at $\alpha^2 = 0{\cdot}75$, $St = 0{\cdot}01$, $L = 8$ and $D = 5$. (*a*) $t = 0{\cdot}15$; (*b*) $t = 0{\cdot}25$; (*c*) $t = 0{\cdot}5$; (*d*) $t = 0{\cdot}55$; (*e*) $t = 0{\cdot}75$; (*f*) $t = 0{\cdot}95$.

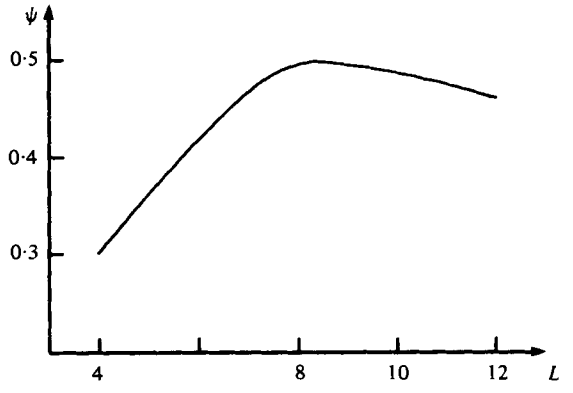


FIGURE 16. Variation of vortex strength at $t = 0{\cdot}5$ with furrow length, calculated for $\alpha^2 = 0{\cdot}75$, $St = 0{\cdot}01$ and $D = 2$.

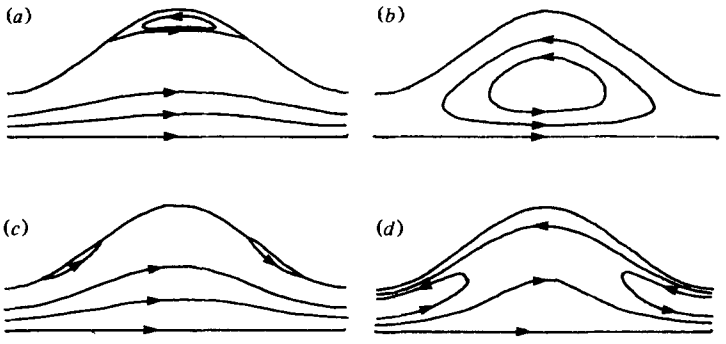


FIGURE 17. Streamlines for viscous flow. $\alpha^2 = 0{\cdot}075$; (*a*) $t = 0{\cdot}45$; (*b*) $t = 0{\cdot}5$; $\alpha^2 = 7{\cdot}5$; (*c*) $t = 0{\cdot}39$; (*d*) $t = 0{\cdot}5$.

when $L \approx 4D$. In figure 16 we have plotted the vortex strength at the instant of zero mean flow against the length of the furrow at constant depth ($D = 2$). It is clear that both the steady and unsteady calculations indicate that a furrow length to depth ratio of 4 will give the strongest vortices in the furrows and if we suppose that strong vortices give good mixing then the choice of dimensions made by Bellhouse *et al.* (1973) is probably near optimum.

### 4.4. *The importance of viscous effects*

In § 4.2 we indicated that the region in which strong vortices occur is primarily one in which the flow structure is dominated by inertial effects. In this section we shall consider the region in which viscous effects are of dominant importance. Our evidence for this comes from solutions of the unsteady Stokes equations of motion obtained by deleting the nonlinear inertial terms in our numerical scheme. The study of the viscous equations has a long history, particularly the study of oscillatory flow past a wavy surface. Yet the main purpose of previous studies [see, for instance, Lyne (1971) and Hall (1973)] has been the steady streaming induced by oscillatory motion past wavy surfaces. We do not consider the steady streaming problem but present the instantaneous streamlines for both Stokes flows and for flows where the inertial terms are small but not negligible. These do not appear to have been set down before.

If the pulsatile Reynolds number is small then the flow develops during the acceleration as a streaming motion through the channel. As the flow decelerates the slower-moving fluid near the wall is influenced most and flow reversal occurs near the apex of the furrow. In the last stages of the deceleration the separated region enlarges as fluid flows backwards along the wall with a pattern similar to that found in inertially dominated flows. In fact the vortex strength in this case (figure 17) is 0·026, more than an order of magnitude less than the vortex strength of an inertially dominated flow. At large values of the pulsatile Reynolds number the flow pattern changes, separation occurring near the strut (figure 17*c*). The continued deceleration results in a recirculation region about the strut (figure 17*d*). The line of separation for Stokes flow can also be obtained and in figure 18 we see that $t_s$ decreases to a minimum near $\alpha^2 = 0{\cdot}6$ and increases slowly thereafter. The flow never separates during the acceleration and this curve should be the limit $St \to \infty$ of the function $t_s(\alpha^2, St)$.

The importance of viscosity in the full Navier–Stokes equations is shown most clearly by calculating solutions at equivalent values of the parameter $\alpha^2$. In figure

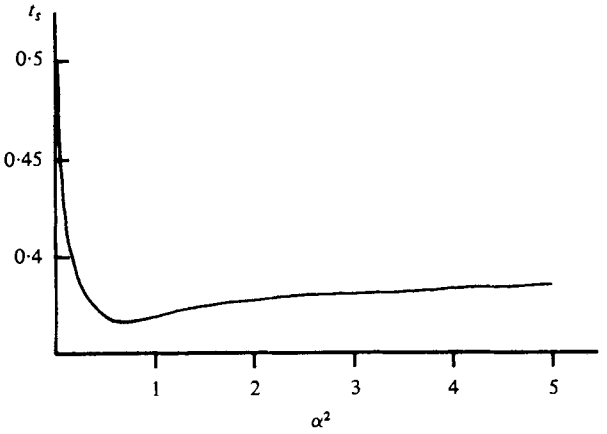


FIGURE 18. Time of flow reversal for viscous flow, calculated for a sinusoidal furrow with $L = 8$ and $D = 2$.

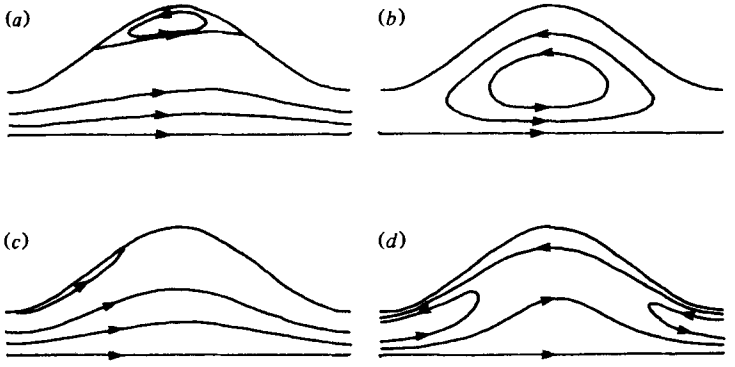


FIGURE 19. Streamlines for solutions to the full Navier–Stokes equations $\alpha^2 = 0{\cdot}075$; $St = 0{\cdot}02$; (*a*) $t = 0{\cdot}45$; (*b*) $t = 0{\cdot}5$; $\alpha^2 = 7{\cdot}5$; $St = 1$; (*c*) $t = 0{\cdot}39$; (*d*) $t = 0{\cdot}5$.

19(*a*) and 19(*b*) we show the flow streamlines when $\alpha^2 = 0{\cdot}075$ and $St = 0{\cdot}02$. Here the Reynolds number is 3·75 and this is outside the vortex mixing region described in §4.1. Clearly the flow could well be approximated by the solutions to the unsteady Stokes equations presented in figure 17(*a*) and (*b*). At a larger value of the pulsatile Reynolds number, $\alpha^2 = 7{\cdot}5$ and $St = 1$, the flow patterns are again similar to those obtained from the Stokes equations (figure 19*c* and 19*d*). Apart from a slight asymmetry introduced by the inertial terms the flow patterns are identical.

## 5. Flow in the Oxford membrane oxygenator

### 5.1. *Basic flow patterns*

Regardless of whether the boundary geometry is sinusoidal or a series of furrows formed by arcs of circles the flow structure remains the same. Thus the ideas given in the preceding two sections are immediately applicable to the design of mass transfer devices using vortex mixing. Here we shall briefly demonstrate the closeness of the structure by giving the streamlines at identical times to those of figure 11 for a geometry typical of a membrane oxygenator. In figure 20 we show the streamlines for

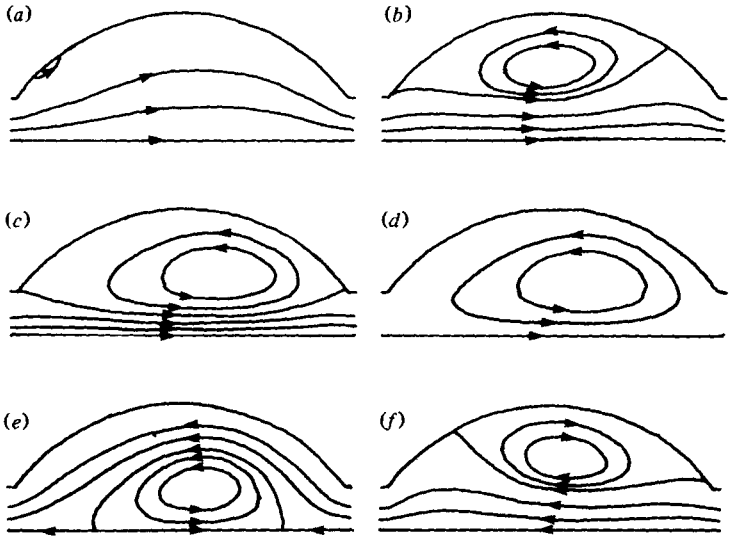


FIGURE 20. Streamlines for unsteady flow through a furrow whose shape is an arc of a circle. Calculated for $\alpha^2 = 0{\cdot}75$, $St = 0{\cdot}01$, $L = 8$, $D = 2$ and $x_w = 0{\cdot}255$. (*a*) $t = 0{\cdot}1$; (*b*) $t = 0{\cdot}25$; (*c*) $t = 0{\cdot}45$; (*d*) $t = 0{\cdot}5$; (*e*) $t = 0{\cdot}55$; (*f*) $t = 0{\cdot}75$.

a furrows channel in which $L = 8$ and $D = 2$ where in addition there is also a finite width to the 'strut' which could support a membrane forming the semicircular furrow. We have arbitrarily chosen the strut width to be 0·255. It can be seen that separation occurs at approximately the same time as for a sinusoidal wall and during the acceleration phase a small separated region forms in the upstream part of the furrow. During the deceleration the separated region enlarges and as the mainstream reverses the vortex is ejected from the furrow. We propose that the vortex formation and the subsequent behaviour of the vortex as the flow reverses results in the devices of Bellhouse *et al.* (1973) having high performance. During the acceleration fluid from the mainstream is moved into the hollow. The formation and growth of the vortex in the furrow results in good mixing of fluid within the furrow and should result in a higher mass transfer rate through the membrane than if diffusion processes alone acted. Then as the mainstream reverses the vortex is ejected from the furrow and there will be good mixing between the fluid in the furrow and the mainstream fluid. In this process it is vital that a strong vortex forms in the furrow and the mainstream flow reverse, displacing the vortex into the mainstream.

### 5.2. *Time of separation*

In the design of high efficiency mass transfer devices it is important to know the critical Reynolds number at which vortex mixing occurs. We have seen in § 4.2 that the time of separation changes dramatically at the critical Reynolds number as the flow characteristics change from viscous dominance to inertial dominance. To demonstrate how the critical Reynolds number varies we show in figure 21 the time of separation for three configurations. If $L = 8$ and $D = 2$ with a strut width of 0·51 the critical Reynolds number lies just below 5 in close agreement with the value obtained for sinusoidally varying channels. If now the depth of the furrow is decreased, to $D = 1{\cdot}5$ the critical Reynolds number increases to a value just below 8. If on the other hand the length

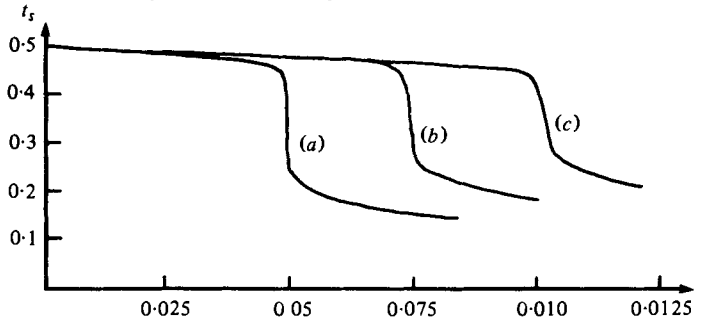


FIGURE 21. Time of separation *versus* $\alpha^2$ for various configurations (*a*) $L = 8$, $D = 2$, $x_w = 0{\cdot}225$; (*b*) $L = 8$. $D = 1{\cdot}5$, $x_w = 0{\cdot}255$; (*c*) $L = 4$, $D = 1$, $x_w = 0{\cdot}1275$, calculated for $St = 0{\cdot}01$.

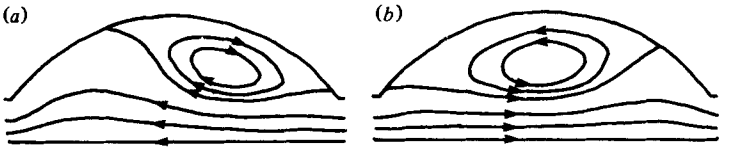


FIGURE 22. Oscillatory flow with a small mean flow component ($\bar{q} = 0{\cdot}1$), calculated at $\alpha^2 = 0{\cdot}75$ and $St = 0{\cdot}01$. (*a*) $t = 0{\cdot}75$; (*b*) $t = 1{\cdot}25$.

and depth are halved to $L = 4$ and $D = 1$ the critical Reynolds number increases to a value near 10. The changes in the critical Reynolds number are consistent with the idea that a change in configuration which reduces the likelihood of separation will increase the Reynolds number that must be achieved in order to have vortex mixing in a channel.

### 5.3. *Effect of mean flows*

In a practical mass transfer device there will be a mean flow superimposed on an oscillatory flow. Bellhouse *et al.* (1973) indicate that they used a mean flow of less than a tenth the peak flow. It is important to know how a mean flow component affects the flow structure described above. We have modified the boundary condition on the stream function to

$$\psi|_{z=1} = \begin{cases} \sin 2\pi t & 0 < t < 0{\cdot}25, \\ \bar{q} + (1-\bar{q}) \sin 2\pi t & t > 0{\cdot}25, \end{cases}$$

in order to simulate a mean flow component. Thus there is a mean flow $\bar{q}$ with a superimposed oscillatory flow of strength $(1-\bar{q})$.

If $\bar{q}$ is small our calculations show that the basic mixing mechanism is likely to remain unaltered. In figure 22 we show the stream function at $t = 0{\cdot}75$ (peak reverse flow) and $t = 1{\cdot}25$ (peak forward flow) for $\bar{q} = 0{\cdot}1$ at $\alpha^2 = 0{\cdot}75$ and $St = 0{\cdot}01$. In the reverse flow cycle the vortex strength is reduced from 0·23 at peak forward flow to 0·15 at peak reverse flow but the basic flow mechanism clearly remains. In this case it would be appropriate to ensure that the peak Reynolds number of the reverse flow cycle is sufficient to cause vortex mixing. Alternatively if $\bar{q}$ is large then small pulsations superimposed on a relatively large mean flow do not displace the vortex from the furrow. In figure 23 the stream function is shown at the maximum and minimum flow and the only difference is that at minimum flow the vortex strength is 0·12 whereas at peak flow it is 0·15. When the mean flow is of the same order as the oscillatory component interesting effects occur. In figure 24 we show the case $\bar{q} = 0{\cdot}55$ when the

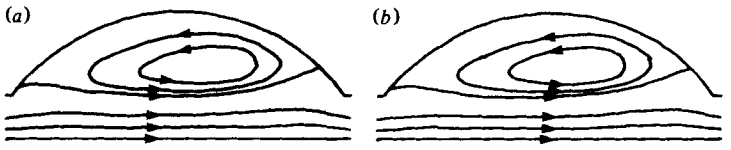


FIGURE 23. Oscillatory flow with a large mean flow component ($\bar{q}=0{\cdot}9$), calculated at $\alpha^2=0{\cdot}75$ and $St=0{\cdot}01$. (*a*) $t=0{\cdot}75$; (*b*) $t=1{\cdot}25$.

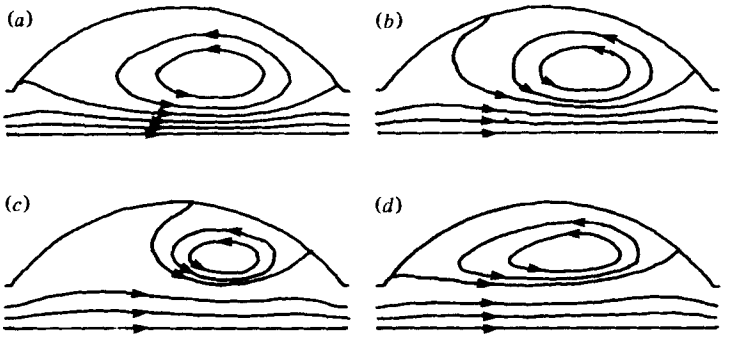


FIGURE 24. Oscillatory unidirectional flow ($\bar{q}$ = 0·55) streamlines calculated for $\alpha^2$ = 0·75 and $St$ = 0·01. (*a*) $t$ = 0·75; (*b*) $t$ = 0·8; (*c*) $t$ = 0·85; (*d*) $t$ = 1·25.

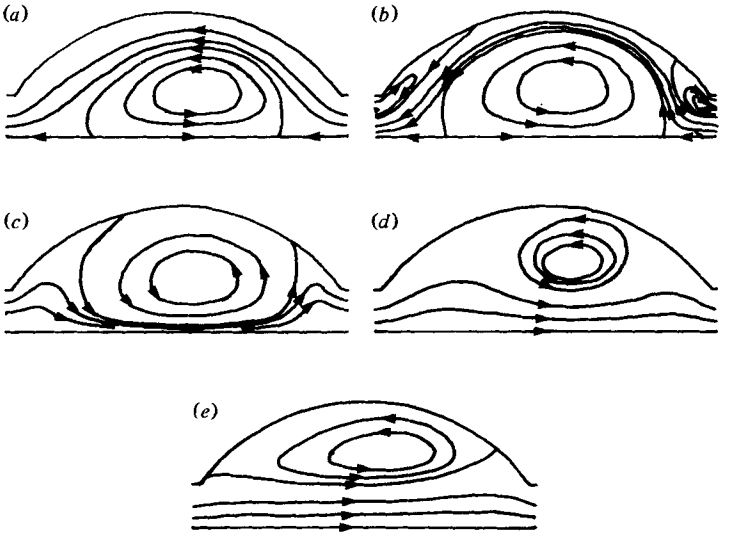


FIGURE 25. Oscillatory flow that just reverses ($\bar{q}$ = 0·45), calculated at $\alpha^2$ = 0·75 and $St$ = 0·01. (*a*) $t$ = 0·75; (*b*) $t$ = 0·84; (*c*) $t$ = 0·86; (*d*) $t$ = 0·9; (*e*) $t$ = 1·25.

oscillation will have magnitude 0·45. This flow is unidirectional but with large changes in magnitude of the flow rate. In figure 24(*a*) at time $t$ = 0·75, the instant of minimum flow, the vortex has grown to fill the furrow and bulges to the membrane. As the flow accelerates fluid flows into the upstream part of the furrow and begins to displace the vortex. As this process continues the vortex is eliminated from the furrow (figure 24*b* and 24*c*) and a new vortex is established in the furrow, shown in figure 24(*d*) at the instant of peak flow. If on the other hand the mean flow is small enough so that the flow just reverses the flow structure is even more complex. Suppose that a vortex

has been set up in the furrow whilst the fluid is flowing forwards. As the flow decelerates the vortex enlarges and the reversal of the fluid flux causes the vortex to be ejected from the furrow (figure 25*a*). Then the reverse flux begins to decrease and a second separated region occurs about the strut (figure 25*b*). The similarity of this with the large $\alpha^2$ behaviour of viscous-dominated flows leads us to suggest that the second separated region is essentially a viscous phenomenon caused by the deceleration of the reverse flux. As the flux becomes positive the main vortex reattaches to the wall (figure 25*c*) but continued acceleration of the mainstream lifts that vortex from the wall (figure 25*d*) and eventually it is eliminated. The mainstream then separates and a new vortex forms in the furrow (figure 25*e*).

The complicated flow patterns that occur when a mean flow component is superimposed on an oscillatory component make it difficult to give a simple explanation of mixing processes in such flows. If the mean flow component is small then the pattern of § 5.1 is retained and convective mixing could still be achieved through vortex formation in the furrow and ejection into the mainstream. If the mean flow is large the vortex just pulsates in the furrow, there is little exchange between the mainstream and the furrow and we should not expect the mixing to be as efficient as if the mean flow was small. Between these two mean flow rates there is a region where the flow patterns make it impossible to decide *a priori* whether high or low convective mixing would be attained.

## 6. Conclusions

In dealing with a topic as complicated as the structure of solutions to the unsteady Navier–Stokes equations it is difficult to be both all encompassing and concise. We have attempted to show some of the details of the solutions which we believe are of relevance to an arbitrary oscillatory flow. Further we have only considered variation of the governing parameters about values of interest in the design of high performance mass transfer devices. There are two areas of major importance that we have not covered. Firstly the region in which quasi-steady theory does not hold during the acceleration, yet the flow development is still primarily controlled by inertial effects. In terms of § 4 this is the region in which the Strouhal number varies between 0·02 and 0·1. The second region we have ignored is given by large values of the pulsatile Reynolds number. We would expect that at large Reynolds numbers the flow would be turbulent and presumably on the plot of $\alpha^2$ *vs.* *St* there will be a second line other than that which divides laminar inertially generated vortices from viscous-dominated flows, a line that divides laminar vortices from turbulent motion. More likely there will be a region in which unsteadiness other than the imposed oscillation is evident and in which turbulence occurs as the pulsatile Reynolds number increases. Clearly many facets of the solution structure remain undiscovered.

We have shown that for steady flow there is a critical Reynolds number that must be attained for the flow to be separated. In unsteady flow, for small Strouhal numbers the flow development during an acceleration occurs in a quasi-steady manner. In order to have vortex mixing the peak Reynolds number must be sufficient to cause an equivalent steady flow to separate. The high efficiency of the devices of Bellhouse *et al.* (1973) is explained by a two-part cycle in which mixing occurs within the furrow and then between the furrow and the mainstream. A small mean flow superimposed

on an oscillation will have little effect on this mechanism. During a deceleration a separated region behaves in a distinctly non-quasi-steady manner and great care is needed in applying quasi-steady theory to a separated flow. In a companion paper (Stephanoff *et al.* 1980) experimental evidence is presented which confirms the results presented here.

I am indebted to Professor Sir James Lighthill for guidance and criticisms during the preparation of the manuscript. I thank Dr T. J. Pedley and Dr B. J. Bellhouse for invaluable discussions. This work was supported by the Science Research Council and the Wolfson Foundation.

## REFERENCES

BELLHOUSE, B. J., BELLHOUSE, F. H., CURL, C. M., MACMILLAN, T. I., GUNNING, A. J., SPRATT, E. H., MACMURRAY, S. B. & NELEMS, J. M. 1973 *Trans. Amer. Soc. Artif. Int. Organs* **19**, pp. 77–79.

BELLHOUSE, B. J., BELLHOUSE, F. H. & HAWORTH, W. S. 1977 *European Soc. Artif. Organs* **4**, (in the press).

BELLHOUSE, B. J. & SNUGGS, T. A. 1977 *Inserm-Euromech* 92, **71**, 371–384.

GILLANI, N. V. & SWANSON, W. M. 1976 *J. Fluid Mech.* **78**, 99–127.

HALL, P. 1974 *J. Fluid Mech.* **64**, 209–226.

LIGHTHILL, M. J. 1963 *Laminar Boundary Layers* (ed. L. Rosenhead), chap. 2. Oxford University Press.

LYNE, W. H. 1971 *J. Fluid Mech.* **50**, 33–48.

ROACHE, P. J. 1972 *Computational Fluid Dynamics*. Hermosa.

SMITH, F. T. 1974 *J. Inst. Math. Appl.* **13**, 127.

SMITH, F. T. 1976 *Quart. J. Mech. Appl. Math.* **29**, 343–364.

SNUGGS, T. A. 1977 D.Phil. Dissertation. Oxford University.

STEPHANOFF, K., SOBEY, I. J. & BELLHOUSE, B. J. 1980 *J. Fluid Mech.* **95**, 27–32.

STEWARTSON, K. & WILLIAMS, P. G. 1969 *Proc. Roy. Soc.* A **312**, 187–206.